

Soft Matter

Accepted Manuscript



This is an *Accepted Manuscript*, which has been through the Royal Society of Chemistry peer review process and has been accepted for publication.

Accepted Manuscripts are published online shortly after acceptance, before technical editing, formatting and proof reading. Using this free service, authors can make their results available to the community, in citable form, before we publish the edited article. We will replace this *Accepted Manuscript* with the edited and formatted *Advance Article* as soon as it is available.

You can find more information about *Accepted Manuscripts* in the [Information for Authors](#).

Please note that technical editing may introduce minor changes to the text and/or graphics, which may alter content. The journal's standard [Terms & Conditions](#) and the [Ethical guidelines](#) still apply. In no event shall the Royal Society of Chemistry be held responsible for any errors or omissions in this *Accepted Manuscript* or any consequences arising from the use of any information it contains.



The Mechanoelectrical Response of Droplet Interface Bilayer Membranes

Received 00th January 20xx,
Accepted 00th January 20xx

DOI: 10.1039/x0xx00000x

www.rsc.org/

E.C Freeman^a, J. S. Najem^b, S. Sukharev^d, M.K. Philen^c, D.J. Leo^a

Mechanotransduction and interfacial properties in unsupported liquid biomimetic membranes are explored using the droplet-interface bilayer technique. The fluidic monolayer-membrane system afforded by this technique allows for dynamic control over the membrane dimensions and curvature, which under periodic deformations generates capacitive currents (akin to a Kelvin probe), and permits a detailed electrostatic characterization of the boundary layers as well as observation of flexoelectric effects. Both high and low displacement frequency regimes are examined, and the results show that the mechanoelectric signals generated by the membranes may be linked to the membrane electrostatic structure. In addition, we show that periodic membrane bending in a high-frequency regime generates tension sufficient to activate reconstituted mechanosensitive channels.

Introduction

The droplet-interface bilayer (DIB) technique described by Bayley *et al.*^{1,2} and Funakoshi *et al.*³ provides a cell membrane-like scaffold for the reconstitution of functional elements such as ion channels, pumps and transporters. This technique uses lipids as a surfactant in water-in-oil emulsions, wherein aqueous droplets are deposited inside an oil reservoir with lipids dissolved in either fluid phase (Figure 1)⁴. These lipids are amphiphilic, possessing a hydrophobic tail and hydrophilic head. Consequently, the lipids coat the aqueous droplets at their oil-water interfaces, arranging their head groups in the aqueous phase as their hydrocarbon tails extend out into the oil. Once these lipid monolayers have formed on the droplet surfaces, the droplets may be manipulated into contact, either manually², through microfluidic chips^{5,6}, or through controlled printing schemes⁷. The lipid monolayers expel the oil between the droplets at the points of contact and draw together into stable lipid bilayer membranes, separating the connected droplet interiors. These membranes approximate naturally occurring membranes and provide a suitable scaffold for the reconstitution of complex biomolecules such as transporters and channels⁸, providing pathways for exchange between the droplets. As an extension from the unit to the 'systems' level, the DIB technique allows for the creation of complex microfluidic membrane architectures and networks through the placement and connection of multiple droplets. These

droplets may be arranged into various configurations for advanced studies such as signal rectification⁹ or osmotic actuation⁷.

The DIB system is entirely fluidic – the membrane is able to exist freely in an oil reservoir without requiring a scaffold or solid partitioning with an aperture. A single DIB droplet pair consists of three phases and two boundaries – the two aqueous droplets, the surrounding oil, the lipid monolayers coating the aqueous droplets and the lipid bilayer connecting the two droplets. The functional region of interest is the thin bimolecular membrane between the droplets surrounded by a meniscus whose variable configuration defines the boundaries of the bilayer (Figure 1.b). The membrane characteristics are dynamic¹⁰, and the membrane may grow and shrink in response to mechanical constraints or perturbations¹¹. This opens up new avenues of mechanotransduction in DIB membranes^{12, 13}, wherein the droplet-membrane system is capable of generating an electrical signal when subjected to mechanical perturbation^{12, 14-18}, dubbed the mechanoelectric current. This is accomplished through the elasticity of the DIB emulsions¹⁹, transferring the displacement of constitutive droplets into deformation of the interfacial membranes.

Overview of the Research Objectives and Approach

The primary objective of this research is the characterization of the mechanoelectrical response of the DIB membranes. This is achieved through the axial oscillation of the constitutive droplets at fixed frequencies and magnitudes in a shielded, low-noise, voltage-clamped environment. Droplets are suspended from hydrogel anchors inside rigid capillary tubes, providing precise mechanical manipulation. Silver-silver

^a College of Engineering, University of Georgia.

^b Department of Mechanical Engineering, Virginia Tech

^c Department of Aerospace and Ocean Engineering, Virginia Tech

^d Department of Biology, University of Maryland

chloride (Ag/AgCl) electrodes embedded in the hydrogels provide reliable electrical connection to the droplet interiors. One droplet is fixed in place as the second droplet is actuated; mimicking a controlled displacement of a single droplet contained within a DIB network pair. The adjustable experimental parameters are the size of the constitutive

droplets, the magnitude of the applied axial displacement, the frequency of the applied axial displacement, and the magnitude of the supplied transmembrane potential. The generated mechano-electrical current is recorded through an amplifier operating in voltage-clamp mode.

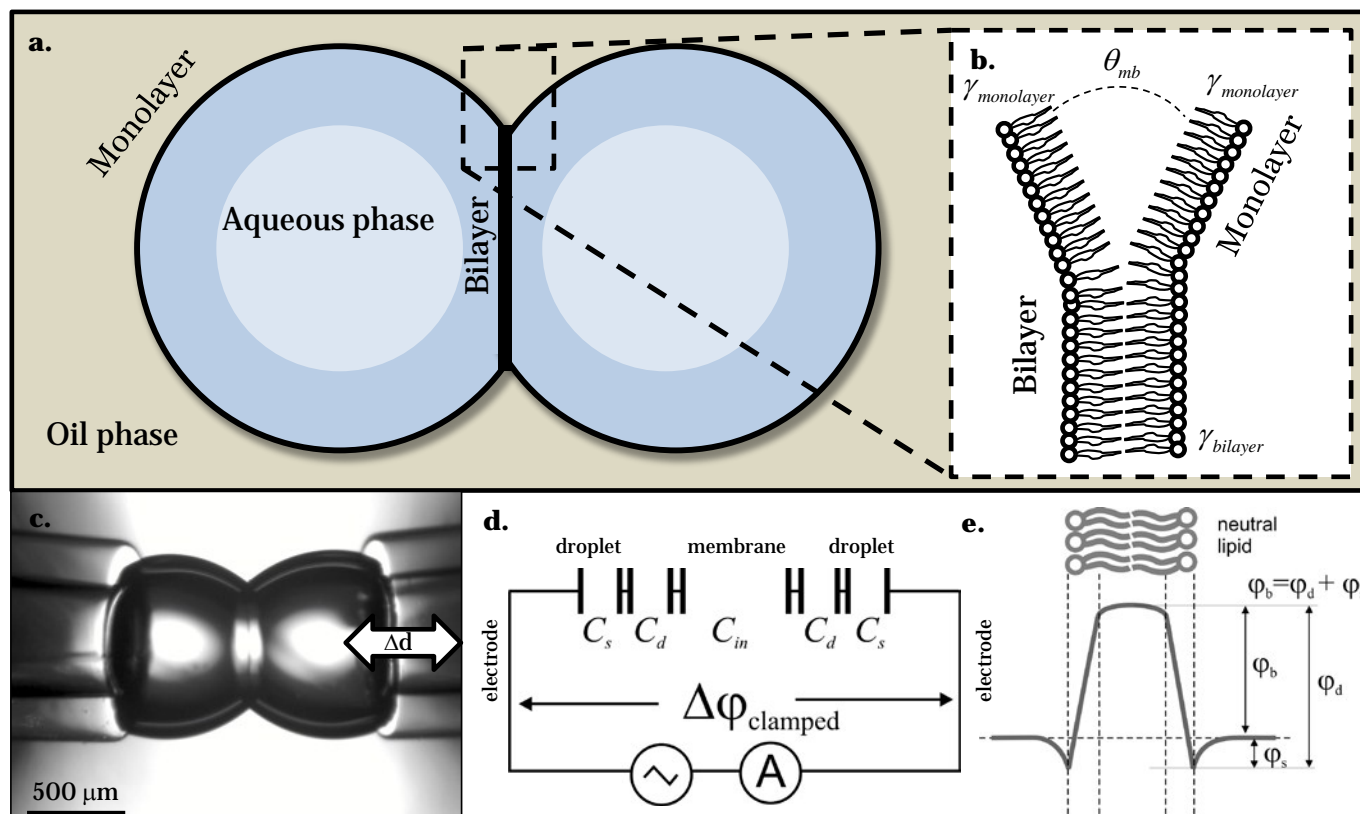


Figure 1 – The Droplet-Interface Bilayer technique¹ applied to mechano-electricity. a) Liposome-containing aqueous droplets are deposited into an oil reservoir, allowing lipid monolayers to assemble on their surface. When the droplets are brought into contact, the lipid monolayers adhere together in a lipid bilayer, often approximated as a capacitor. b) The contact angle at the monolayer-bilayer meniscus is determined by the balance of the tension between the two interfaces, and the membrane dimensions may be controlled through the meniscus configuration. c) Droplet compression and separation is achieved by attaching the droplets to hydrogels cured within capillary tubes, altering the meniscus and mechanically exciting the interfacial membrane. d) On a macroscopic scale, this results in a change in the membrane capacitance, where the membrane is approximated as a combination of capacitors, with a low-capacitance hydrophobic core C_{in} . However, the membrane electrostatics are more complex, and contain an internal electrostatic potential profile that will also play a role in the mechano-electric signal including surface ϕ_s and dipole ϕ_d potentials comprising the total boundary potential ϕ_b . e) In a symmetric membrane, the boundary potentials are equivalent.

The bilayer lipid membrane itself acts as a natural capacitor²⁰. Perturbing the structure of the membrane through mechanical displacement produces a mechano-electric current proportional to the transmembrane potential and the rate of change in the membrane capacitance^{12, 13}. This has been modelled as a capacitive current, stemming directly from the traditional capacitor model for cellular membranes^{20, 21} (Figure 1.d). However the membrane contains multiple layers each possessing internal electrostatic components (Figure 1.e) that are not included in this capacitor model²²⁻²⁴. Interactions between charges on the surface of the membrane and the surrounding electrolyte create a diffuse electrical double layer characterized by the surface potential ϕ_s . The internal dipole potential ϕ_d originates from anisotropic structure of the headgroup region and oriented water at the polar-apolar

interface^{25, 26}. In a symmetric membrane ϕ_d and ϕ_s on both sides of the membrane are equivalent, leading to matching ϕ_b values at the boundaries through symmetric potential profiles. For these symmetric membranes, the transmembrane potential ϕ_{clamp} supplied by the amplifier is directly translated into a potential drop across the hydrophobic core ϕ_{in} . The specific capacitance of the hydrophobic core C_{in} is much lower than the capacitance of the dipole C_d and surface C_s regions, and it may be safely assumed that the majority of the clamped potential ϕ_{clamp} drops across the hydrophobic slab. The dimensions (primarily area) of the membrane's hydrophobic core are altered through mechanical perturbation and are expected to change the capacitance and generate displacement currents sensitive to the asymmetry of pre-

existing charges and dipoles in the membrane, exactly as in a miniature Kelvin probe^{27, 28}.

The link between the membrane dimensions and mechanical constraints have been explored previously^{10, 11}. The bilayer dimensions are a balance of normal pressure acting at the droplets, tension in each monolayer and cohesive forces created by expulsion of the organic solvent from the contact between monolayers. The combination of these factors generates tension at the monolayer-bilayer meniscus (Figure 1.b). In a completely unconstrained system, the droplets will maintain a near-spherical morphology and their shared equilibrium bilayer size will be governed by a combination of the bilayer and monolayer tensions, growing until the tensions at the meniscus are balanced. If the droplet geometries are altered through mechanical constraints or forces, the angle at the meniscus is changed and tension is added or removed from the bilayer membrane. Consequently the membrane will grow or shrink until a new equilibrium is reached.

Results and Discussion

First, the response of the DIB membrane to axial compression and separation of the droplets must be characterized. As the droplets are mechanically perturbed through compression or separation, the bilayer dimensions will change accordingly and these changes may be observed through the experimentally

recorded current. The capacitive current for a variable capacitor may be written as follows:

$$i_{\text{capacitive}} = \underbrace{C_{in} \frac{d\varphi_{in}}{dt}}_{\text{elec}} + \underbrace{\varphi \frac{dC_{in}}{dt}}_{\text{mech}} \quad (1)$$

The first component on the right hand side of this equation is the traditional capacitive current. The capacitance of the membrane C_{in} is often measured using a low-amplitude triangle wave voltage (10 mV, 10 Hz), providing a constant $d\varphi_{in}/dt$. Step functions in axial compression and separation are applied to the droplets, providing changes in the interfacial dimensions through membrane growth and reduction. The frequency of the applied oscillating transmembrane potential is great enough that the first term of the capacitance current ($C_{in}d\varphi_{in}/dt$) renders the current associated with the simultaneous changes in membrane dimensions ($\varphi_{in}dC_{in}/dt$) negligible in comparison, allowing for isolation of the change in membrane capacitance with respect to time as seen in Figure 2. Here the droplets are compressed and separated as a triangle wave voltage signal is supplied and the corresponding changes in membrane capacitance are plotted. The changes in membrane dimensions with the compression and separation are not immediate, and a relaxation behaviour is observed.

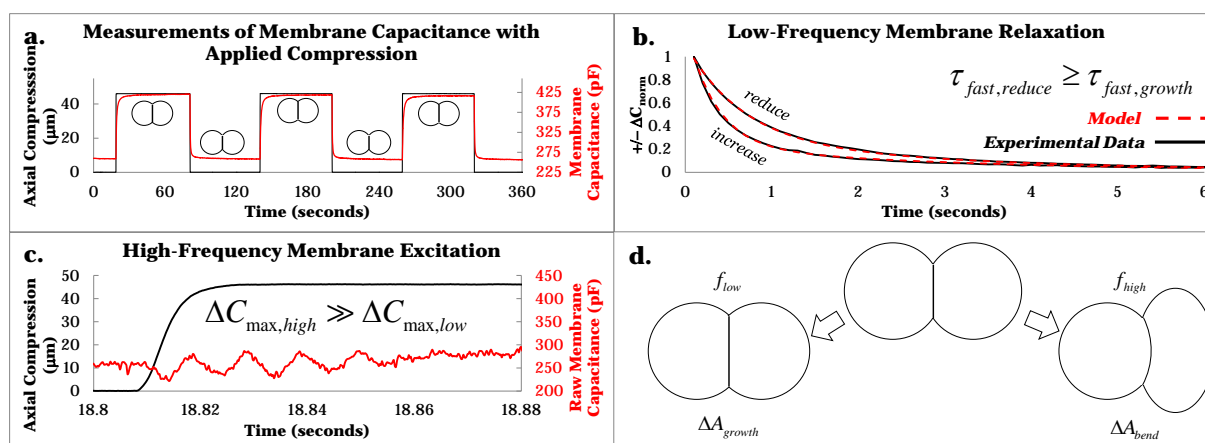


Figure 2 – a) Relaxation of membrane capacitance with an applied step compression and removal, cycling the droplets between the two states. A simultaneous low-voltage triangle wave voltage was applied to measure the membrane capacitance with respect to time during the compression-relaxation cycles. b) The size of the membrane lags behind the applied displacement, leading to characteristic relaxation times for membrane growth and reduction. c) A quickly damped transient signal is observed during the step input, exhibiting a much higher change in capacitance per second and matching a quickly damped transient response of the membrane to the input. d) The membrane responds differently to high and low frequency vibrations.

The membrane response to step displacements may be estimated by fitting the capacitance to two exponential terms, one for the initial response and one for the gradual relaxation as shown in Figure 2.b. C_0 is the capacitance prior to deformation, and C_{shift} is the total change in capacitance after the new equilibrium is reached.

$$C(t) = C_0 + C_{shift} \left[1 - \left(K_{fast} \exp\left(-\frac{t}{\tau_{fast}}\right) + K_{slow} \exp\left(-\frac{t}{\tau_{slow}}\right) \right) \right] \quad (2)$$

Noise and artefacts are smoothed out by breaking the current into segments and taking the average absolute value of the current for each segment then dividing by the constant $d\varphi_{in}/dt$ supplied by the triangle-wave voltage signal. The membrane exhibits a relaxation behaviour with the axial

compression and separation, gradually approaching new equilibrium values and altering back and forth between them reversibly (Figure 2.a). This behaviour may be modelled as a combination of exponential terms as seen in Equation (4) and shown in Figure 2.b. Both the compression and separation stages share the same slow relaxation behaviour, with τ_{slow} of approximately 5-7 seconds. The more rapid initial stage differs slightly between the two, with a τ_{fast} of 0.4 and 0.85 seconds for the separation and compression cycles respectively. These changes in membrane dimensions correspond to the slow bulging regime originally described by Petrov¹⁴, and are present in low frequency vibrations. As the frequency of droplet oscillation increases the mechanoelectric current generated by changes in the membrane's equilibrium dimensions will be reduced drastically - at frequencies above 2 Hz, the observed changes in membrane area are reduced by an order of magnitude²⁹. This component of the mechanoelectric current is limited by the maximum rate of growth for the

membrane, which corresponds to a peak rate of capacitance change of roughly 20 pF/s in this system.

The first component of the capacitive current equation (Equation (1)) allows for the study of the membrane capacitance through a varying electrical signal. The second component of the capacitive current equation allows for the study of the electrostatic profile through the generation of mechanoelectric current, or the current generated by perturbing a charged membrane. With a low-frequency sinusoidal mechanical excitation of the droplets, the DIB system mimics the classical Kelvin probe^{27, 28}. As the membrane capacitance changes with the axial compression and separation (Figure 2.a), an alternating current is generated that scales linearly with the potential drop across the hydrophobic core of the lipid membrane. This is the simplest form of the mechanoelectric current supplied by these DIB membranes, and is derived from Equation (1) and the capacitor model presented in Figure 1.d.

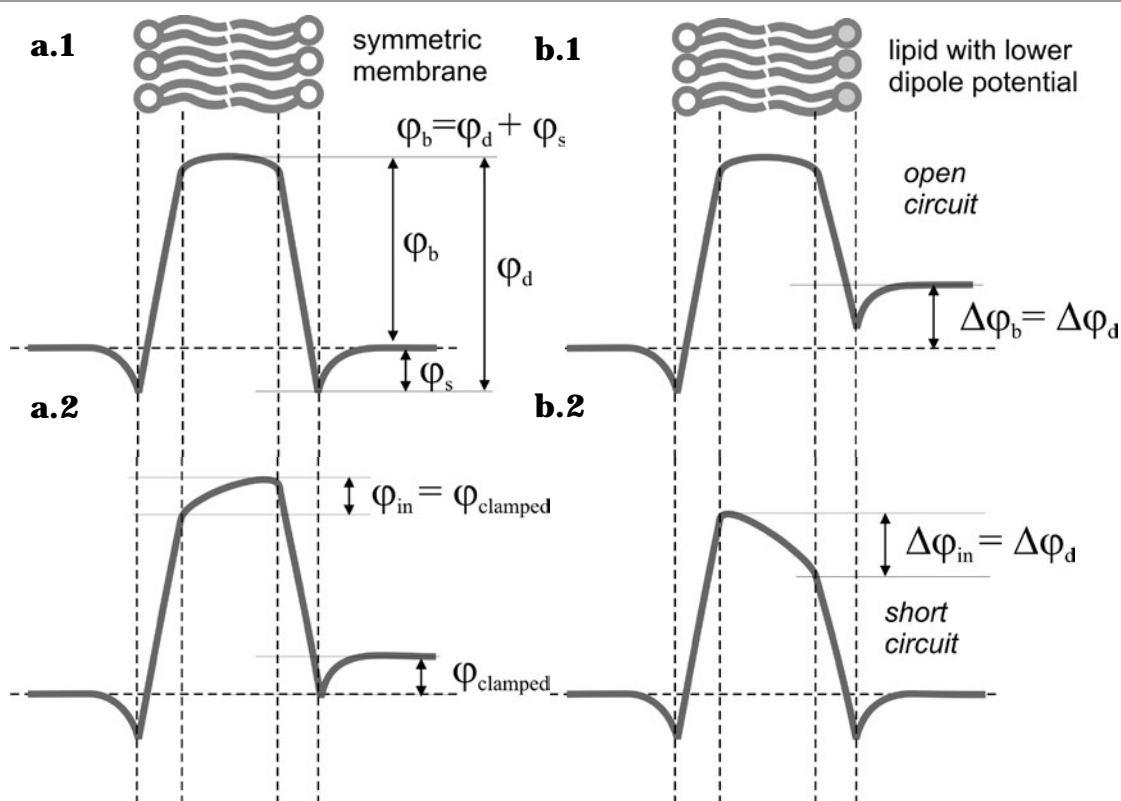


Figure 3 - Relationship between the clamped (or defined) potential and membrane asymmetry. a.1) If the membrane leaflets are symmetric, then the boundary potentials are equal and $\Delta\phi_b$ is zero. a.2) Any clamped potential ϕ_{clamp} will be applied across the membrane interior, and the potential drop across the membrane is equivalent ($\phi_{clamp} = \phi_{in}$). b.1) If the membrane leaflets are asymmetric this leads to a shift in the measured boundary potential $\Delta\phi_b$. b.2) Under short-circuit conditions, this leads to a potential drop across the membrane interior even when ϕ_{clamp} is set to zero ($\phi_{in} = \phi_{clamp} - \Delta\phi_b$).

The resulting current may be used to infer the fine electrostatic structure of the membrane. Typically DIB membranes are symmetric, sharing the same leaflet composition on both sides. As a result the electrostatic profile boundary potentials are cancelled out between the two leaflets, resulting in symmetric boundary potentials at the electrodes ϕ_b (Figure 3).

In an asymmetric membrane the difference between the two leaflets $\Delta\phi_b$ may be non-zero due to different surface charges and/or dipole potentials. The difference in the electrostatic structures $\Delta\phi_b$ leads to a shift in the measured electrode values, and the amplifier compensates for this by providing a transmembrane potential ϕ_{clamp} that corresponds to the asymmetry in the membrane. The equation for capacitive

current (Equation (2)) may be re-written by substituting $\varphi_{clamp} - \Delta\varphi_b$ for φ_{in} :

$$i = C_{in} \frac{d(\varphi_{clamp} - \Delta\varphi_b)}{dt} + (\varphi_{clamp} - \Delta\varphi_b) \frac{dC_{in}}{dt} \quad (3)$$

The mechanoelectric current will be minimized when $\varphi_{clamp} - \Delta\varphi_b = \varphi_{in} = 0$. If the membrane is symmetric, the minimum current will occur at $\varphi_{clamp} = 0$ and the current will be symmetric with respect to the clamped potential, shown in Figure 4. Any deviation from this behaviour at low frequencies of oscillation may be attributed to asymmetry in the membrane. The DIB approach for creating model membranes is well suited for the formation of asymmetric membranes by combining droplets with different compositions of dispersed liposomes³⁰. To demonstrate how the mechanoelectric current may be linked to this asymmetry. To illustrate this concept, asymmetric DIB membranes were created with two leaflet compositions: 1,2 diphytanoyl-sn-glycero-3-phosphocholine (DPhPC) and 1,2-di-O-phytanoyl-sn-glycero-phosphocholine (DOPhPC), an ether form of the lipid. Both of these phospholipids share similar characteristics and are largely compatible; however recent results show a difference in their dipole potentials φ_d between 100 and 200 mV dependent on the area per lipid molecule in the monolayer leaflets³¹.

Asymmetric DIB membranes were created by combining a droplet containing DPhPC liposomes with a droplet containing DOPhPC liposomes. The two droplets were separated for a sufficient period of time for monolayer formation then brought into contact to form an asymmetric lipid membrane at their interface. Immediately after membrane formation the droplets were sinusoidally oscillated at 1 Hz, allowing for the continuous growth and shrinkage of the interfacial membrane as seen in Figure 2.d. The clamped potential was then varied at a low frequency, low enough to ensure that the first component of the mechanoelectric current was minimized in comparison to the second (< 10 mHz). The varying mechanoelectric current with respect to the clamped potential φ_{clamp} was calculated by integrating the peaks contained within the power spectral density (PSD) analysis of segments of the experimental data that corresponded to the oscillation frequency (1 Hz). The mechanoelectric current – voltage relationship may then be examined as seen in Figure 4. This plot is not a traditional I-V plot; the current presented here is the integrated peak in the PSD analysis corresponding to the frequency of oscillation. All plots of the integrated peaks gained from the PSD analysis of experimental data are appropriately labeled “Mechanoelectric Current” rather than “Current.”

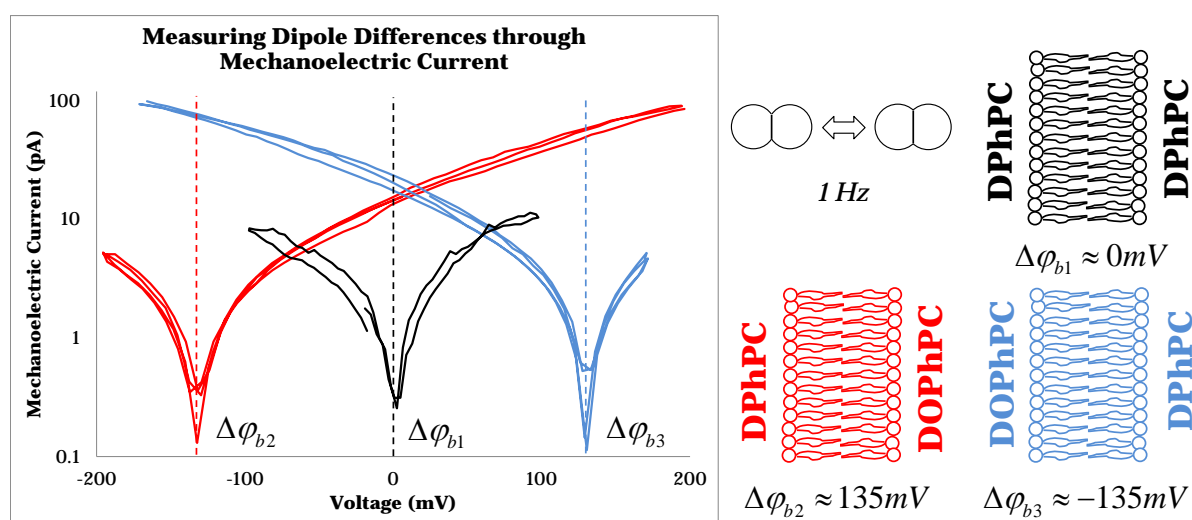


Figure 4 – Mechanoelectric current plotted as a function of voltage for asymmetric membranes of DPhPC and DOPhPC with one symmetric DPhPC case for comparison. The current axis is in log scale to emphasize the locations of the minimum current. The membrane asymmetry leads to an offset in the transmembrane potential with respect to the clamped potential. Swapping the droplet location relative to the source and ground reverses the position of the minimal current where clamped potential exactly offsets the membrane asymmetry.

The results show a minimum mechanoelectric current at ± 135 mV for asymmetric DIB membranes with DPhPC and DOPhPC. At these minimum values for the mechanoelectric current, the clamped potential matches the asymmetric potential, or $\varphi_{clamp} - \Delta\varphi_b = 0$. The rate of change in capacitance (or slope of the mechanoelectric current with respect to potential) for each droplet pair is slightly different due to differences in droplet shapes and size, but the overall result shows clearly that the asymmetry in the membrane is equivalent to a 135 mV difference, matching reported

experimental values for DPhPC and DOPhPC³¹. This demonstrates a unique method for assessing membrane asymmetry through mechanoelectric current.

According to the relaxation constants obtained for membrane growth and wetting, changes in membrane area will be effectively damped out at high frequencies. However it is important to remember that in this mode of membrane excitation the displacement is initially applied to the droplets themselves, which have their own mechanical properties³². As the step displacement is applied a brief distortion of the

droplet's near-spherical oil-lipid-water interface occurs which resolves itself quickly relative to the gradual growth and reduction in the membrane area. This transient droplet distortion is accompanied by a mechano-electrical current, and continuously oscillating the droplets at a high frequency generates a corresponding harmonic mechano-electrical response¹². This harmonic droplet distortion is distributed asymmetrically between the droplets, and the oscillating droplet accommodates the bulk of the distortion. This asymmetric distortion perturbs the membrane by altering the surface orientations at the meniscus (Figure 2.d), and rapid changes in the membrane capacitance are noticeable in the raw data as shown in Figure 2.c. In this high frequency regime the membrane exhibits a much greater response in the capacitive signal than the limited rate of membrane growth and reduction allows (roughly a 400 fold increase in dC_{in}/dt

compared to the low frequency regime). This is likely due to membrane bending, wherein the oscillating asymmetric droplet deformation causes the membrane to rapidly cycle between a planar configuration and a curved configuration, exhibiting an elastic strain and resulting change in capacitance. Interestingly, high-frequency droplet deformation produces an offset in the voltage-current relation similar to those seen in Figure 4 for symmetric membranes, which is linked to the mode of membrane deformation. The membrane bending generates a secondary component of the mechano-electrical current that does not follow the previous capacitive model due to the deformation of fixed charged groups or change of dipole density (Figure 1.e) within the membrane, generating flexoelectricity^{14, 15, 33}. This creates a non-zero component of the mechano-electric current at $\varphi_{in} = 0$, pictured in Figure 5.d.

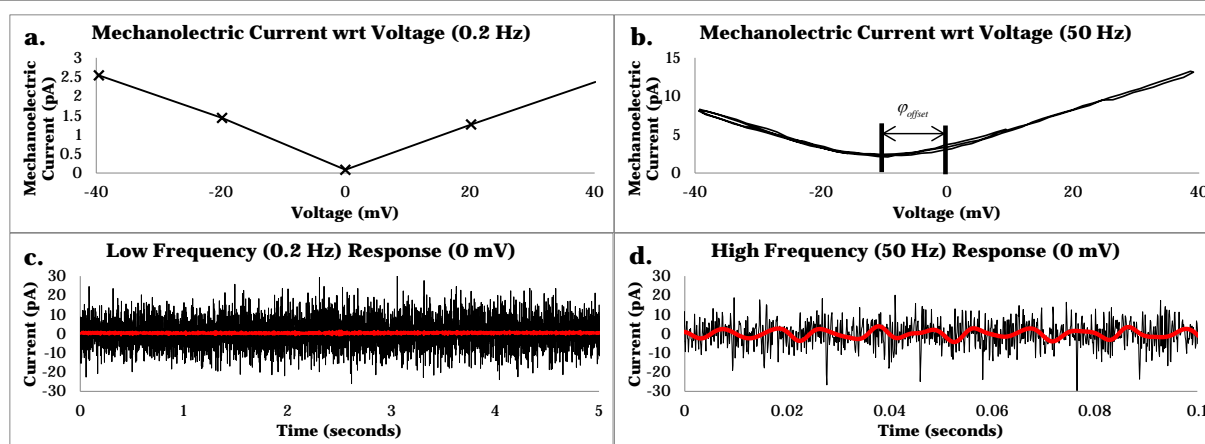


Figure 5 – Switching between low-frequency and high-frequency membrane deformation for symmetric droplets with equal sizes. In low-frequency oscillations, a symmetric membrane produces a mechano-electric current that scales linearly with the clamped transmembrane potential and is symmetric about $\varphi_{in} = 0$. When $\varphi_{in} = 0$, the current is negligible. At high frequencies of oscillation, a secondary current is generated that is not reliant on the supplied transmembrane potential due to flexoelectricity.

The hypothesized flexoelectric component is of particular interest for the development of biomolecular mechanosensors as it may be generated without an external voltage supply and may be activated through the simple displacement of the droplets. This flexoelectricity is traditionally characterized by the flexoelectric coefficient of the membrane f , which predicts the polarization per membrane unit area P_s as a linear function of the membrane principal curvatures ($c_1 + c_2$).

$$P_s = 2f(c_1 + c_2) \quad (4)$$

The flexoelectric coefficient is dependent on the distribution of charged groups on the lipid molecules, orientation of solvating water, and contains contributions from the charges, dipoles and quadrupoles^{14, 17}.

This hypothesized flexoelectric response may be combined with the previous equation for the mechano-electric current. Here φ_{in} is the potential drop across the inner membrane and C_{in} is the capacitance of the membrane's hydrophobic core.

$$i_{membrane} = \underbrace{\varphi_{in} \frac{dC_{in}}{dt}}_{capacitive} + \underbrace{i_{flexo}}_{flexo} \quad (5)$$

When examining the mechano-electric current presented in Figure 5, only the magnitude of the integrated peak is reported, but the form of the flexoelectric and capacitive currents may be examined as well. Three traces were captured from a single experiment encapsulating one oscillation period as shown below in Figure 6 at -10 mV, 0 mV, and 10 mV. The current at 0 mV is selected as the flexoelectric component (negligible contributions from the capacitive component according to Equation (5)) and subtracted from the -10 mV and 10 mV cases to isolate the capacitive component. Initially the experimental data appears to be phase-shifted; however removing the hypothesized flexoelectric current at 0 mV shows similar membrane responses to the single oscillation period. The resulting separated capacitive current shows symmetry about the x axis, further reinforcing the hypothesis that the high frequency membrane deflection contributes its own signal with its own generation mechanics.

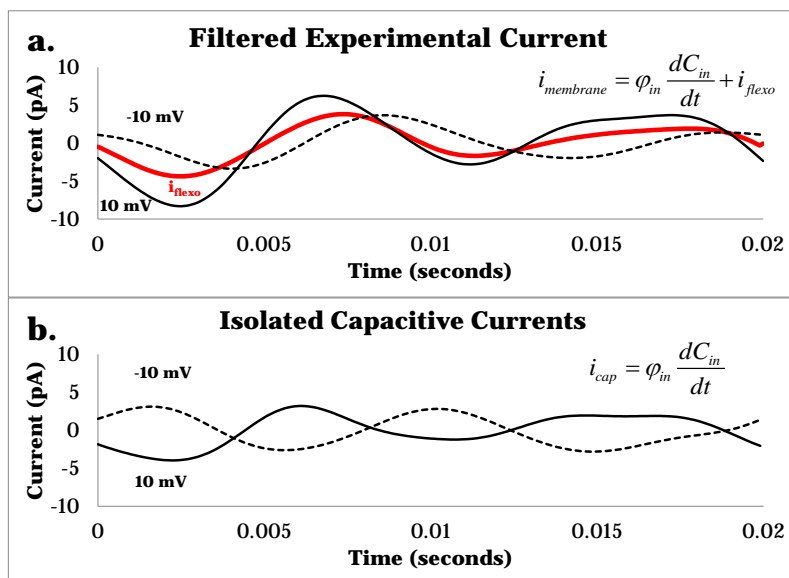


Figure 6 – a) Three traces are captured for an identical oscillation form with symmetric droplets with varying transmembrane potentials (φ_m). In the original traces, no symmetry with respect to the transmembrane potential is present, and the waveforms are distorted due to interference between the flexoelectric and capacitive signals. Subtracting the flexoelectric current restores the expected symmetry with respect to transmembrane potential.

In summary, the membrane exhibits two modes of deformation that are frequency-dependent. At low frequencies of deformation the bilayer accommodates the deformation by zipping the monolayers together at the bilayer-monolayer annulus (Figure 1.b), increasing the membrane surface area and consequently the membrane capacitance¹¹. However, increasing the oscillation frequency shifts the membrane deformation mechanic from gradual growth and reduction to elastic strain and bending, producing flexoelectric current as shown in Figure 5.d in addition to the capacitive current.

Multiple control experiments were conducted to ensure that the signal was a function of the membrane deformation, including cases with a single droplet, disconnected droplets, and droplets in contact without an interfacial membrane, and cases where a third manipulator was used to isolate the ground electrode from the vibrations entirely. In all cases the observed signal was considerably less than the measured signal with the membrane present, and the control signal was never greater than 1 pA. In addition, the noise signals generated in these control cases were out of phase relative to the deformation with the signal generated by membrane deformation.

The offset in the mechanoelectric-voltage relationship may be explained by interference between the two components of the mechanoelectric effect in Equation (5). If the membrane

bending is approximated as the bulging of a spherical cap with curvature c , area A , and central height h , the charge per unit area q/A may be written as a function of the membrane geometry. Differentiating this charge with respect to time provides the experimentally measured current. The membrane thickness is assumed constant with a constant specific capacitance C_s , and the transmembrane potential φ_m is assumed to be constant as well at a prescribed clamped value, nullifying $d\varphi_m/dt$. Neither simplification is wholly accurate, but they allow for a simple mathematical description of the interference between the capacitive and flexoelectric signals. The capacitive current is a function of the change in membrane area, and the flexoelectric current is a function of the charge in membrane curvature (Equation (4)).

$$\begin{aligned} \frac{q}{A} &= C_s \varphi_m + 2fc \\ i_{\text{membrane}} &= \frac{dq}{dt} = C_s \varphi_m \frac{dA}{dt} + C_s A \frac{d\varphi_m}{dt} + 2fA \frac{dc}{dt} + 2fc \frac{dA}{dt} \\ i_{\text{membrane}} &= \underbrace{\varphi_m \left(C_s \frac{dA}{dt} \right)}_{\text{capacitive}} + \underbrace{2f \left(A \frac{dc}{dt} + c \frac{dA}{dt} \right)}_{\text{flexo}} \end{aligned} \quad (6)$$

These two components of the mechanoelectric current are intrinsically linked to the geometry of the membrane, and they may both be described by the central height of the spherical

cap h . Differentiating this value yields the following relationships between the area, curvature, and height:

$$\begin{aligned} h(t) &= \frac{A(t)c(t)}{2\pi} & \frac{dA}{dt} &= \frac{1}{c} \left(2\pi \frac{dh}{dt} - A \frac{dc}{dt} \right) \\ \frac{dh}{dt} &= \frac{1}{2\pi} \left(c \frac{dA}{dt} + A \frac{dc}{dt} \right) & \frac{dc}{dt} &= \frac{1}{A} \left(2\pi \frac{dh}{dt} - c \frac{dA}{dt} \right) \end{aligned} \quad (7)$$

Substituting the equation for the change in curvature with respect to time back into the total membrane current yields the following simplification:

$$i_{\text{membrane}} = \underbrace{\varphi_{\text{in}} \left(C_s \frac{dA}{dt} \right)}_{\text{capacitive}} + 2 \underbrace{f \left(2\pi \frac{dh}{dt} \right)}_{\text{flexo}} \quad (8)$$

For a spherical cap, the area of the cap may be expressed as a function of the planar radii r_{planar} , the cap height h and the membrane flexoelectric coefficient f . Since membrane growth and reduction are minimized at high frequencies, we assume that r_{planar} will remain fixed and any increase in membrane area is a function of elastic strain alone.

$$\begin{aligned} A &= \pi \left(r_{\text{planar}}^2 + h^2 \right) \\ \frac{dA}{dt} &= 2\pi h \frac{dh}{dt} \end{aligned} \quad (9)$$

Substituting this back into the current reduces the equation further, linking the total membrane current to the rate of change in the central deflection:

$$i_{\text{membrane}} = 2\pi \frac{dh}{dt} \left[\underbrace{\varphi_{\text{in}} C_s h}_{\text{capacitive}} + \underbrace{2f}_{\text{flexo}} \right] \quad (10)$$

If we make the assumption that the height of the spherical cap is oscillating following the equation $h = h_{\text{var}} \sin(\omega t) + h_0$, then a final relationship is produced, where h_{var} is the amplitude of oscillation and h_0 is a static offset, or initial displacement:

$$i_{\text{membrane}} = 2\pi\omega \left[\underbrace{\varphi_{\text{in}} C_s \left(h_{\text{var}}^2 \sin(2\omega t) + h_0 h_{\text{var}} \cos(\omega t) \right)}_{\text{capacitive}} + \underbrace{2f h_{\text{var}} \cos(\omega t)}_{\text{flexo}} \right] \quad (11)$$

If h oscillates in a perfectly symmetric fashion about the planar case ($h_0 = 0$), then the two components are independent with the flexoelectric current occurring at the oscillation frequency and the capacitive current occurring at twice the oscillation frequency. This has been shown by Ochs¹⁵ and Petrov¹⁴. If the oscillation is not perfectly symmetric, then constructive or destructive interference occurs dependent on the direction of the static offset in membrane curvature and the magnitude of the applied transmembrane potential. It should be noted that the deformation of the membrane is considerably more complex than this sinusoidal model, but this best illustrates the concept of the interference between the two signal components. The presence of both capacitive and flexoelectric currents will generate constructive or destructive interference dependent on the direction of membrane flexure.

There may be another component to the mechanoelectric current generated at high frequencies. As the droplets deform asymmetrically, their surface area and consequently lipids per area will change as well, assuming that the lateral diffusion rate of the lipids in the interfaces is insufficient to accommodate the rapid droplet deformation. Consequently, both the direction and magnitude of the monolayer tensions entering the bilayer-monolayer meniscus may be affected by the droplet distortion, as the surface tension is directly linked to the lipid density³¹. As the droplet deforms from a spherical configuration to an ellipsoidal configuration its surface area and consequently surface tension will increase, further increasing the asymmetric tension introduced at the meniscus and potentially enhancing the curvature generated in response. The electrostatic potential profile is linked to the lipid density as well³¹, and asymmetric lipid densities in the leaflets comprising the bilayer membrane will generate a transmembrane electrostatic profile similar to the mechanic observed in Figure 4. If the monolayer leaflets contained within the membrane are uncoupled and are able to stretch independently of each other, then this initial imbalance in lipid density may further contribute to the generated mechanoelectric current through an asymmetric electrostatic potential.

To further test the membrane curvature hypothesis, the value for the initial planar offset h_0 was controlled by adjusting the droplet geometries. Droplets are pressurized relative to their surrounding medium, and the pressure inside the droplets ΔP may be expressed as a function of the monolayer surface tension $\gamma_{\text{monolayer}}$ and the radius of the droplet R .

$$\Delta P = \gamma_{\text{monolayer}} \left(\frac{2}{R} \right) \quad (12)$$

Varying the droplet sizes in a DIB pair generates a static pressure imbalance across the interfacial membrane, causing the membrane to swell or bulge out of a planar state and introducing an initial offset curvature in the deformation (R_{bilayer}), allowing for control over the static offset h_0 in the equations above. This may be predicted at equilibrium as a balance of the individual droplet radii R_1 and R_2 and the contact angle at the monolayer-bilayer intersection θ_{mb} ¹⁰.

$$R_{\text{membrane}} = 2 \cos \left(\frac{\theta_{\text{mb}}}{2} \right) \frac{R_1 R_2}{R_1 - R_2} \quad (13)$$

If asymmetric droplet deformation is responsible for the minimum current occurring at negative potentials due to destructive interference between the capacitive and flexoelectric components of the mechanoelectric current, introducing a bias curvature will influence the results by modifying the static offset h_0 . This modifies the interference between the flexoelectric and capacitive currents according to Equation (11), changing the location of the minimum current dependent on the favored direction of membrane curvature. This is confirmed in Figure 7. The interference between the capacitive and flexoelectric currents at the frequency of

oscillation is controllable by tailoring the static curvature in the membrane through droplet dimensions.

A secondary effect may be introduced as well through the altered droplet curvatures. Each droplet possesses an internal pressure according to Equation (12). Smaller droplets are more resistant to deformation and vice versa. Attaching a smaller droplet to the oscillating hydrogel electrode will transmit much

more of the deformation to the stationary droplet, providing a greater change in membrane strain. Conversely, attaching the larger droplet to the oscillating hydrogel will provide a much greater deformation of the droplet surface, leading to engulfing of the smaller stationary droplet into the oscillating droplet and generating a greater flexoelectric current.

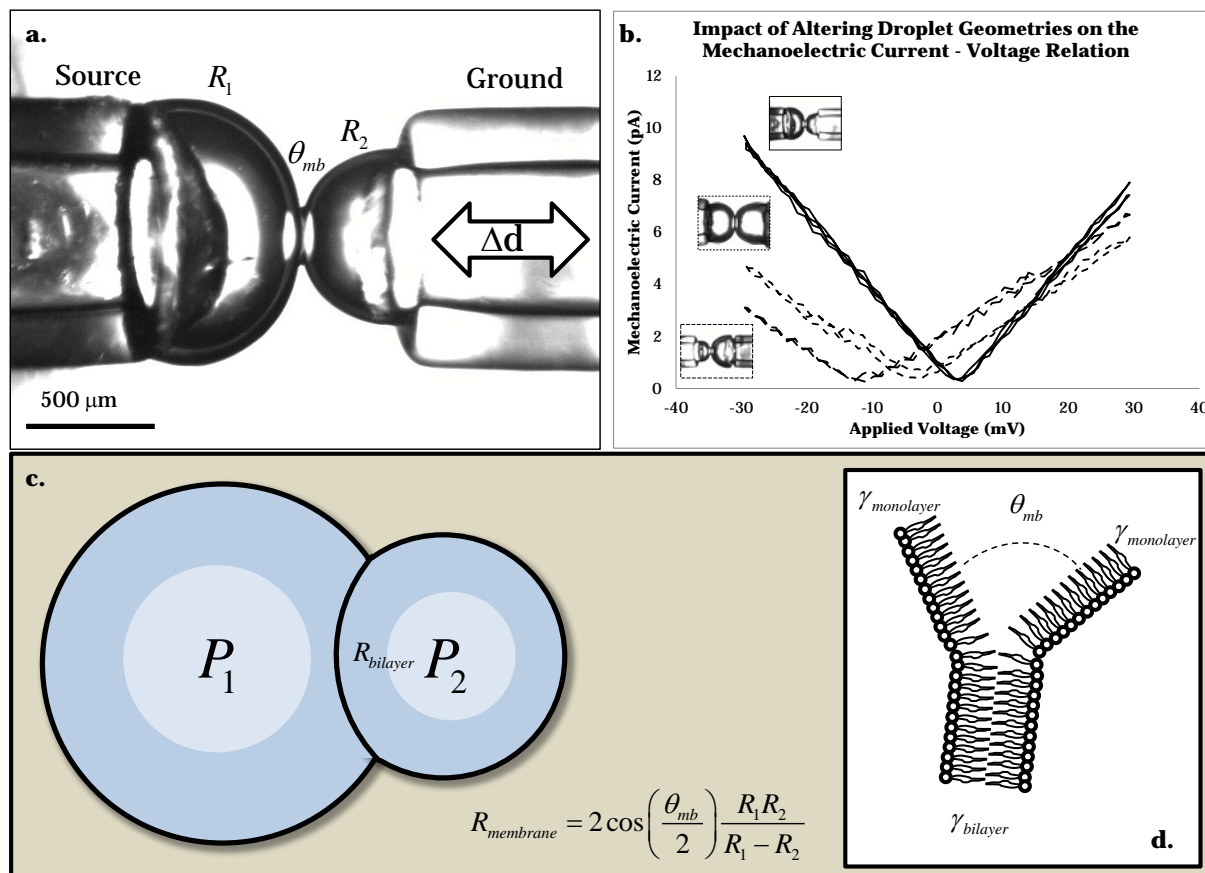


Figure 7 – Impact of altering droplet geometry on the mechanoelectric current. a) A pressure gradient is generated if the droplet sizes are varied, causing the membrane to swell towards the larger droplet. b) As predicted, this alteration in the initial pressure gradient leads to a shift in the location of the minimum current. All oscillations were conducted with a 61.5 Hz sinusoidal signal with a 23 μm displacement. c) Young-Laplace predicts that an initial membrane curvature ρ_0 will develop due to the pressure across the membrane, d) and at equilibrium this curvature may be predicted by the balance of the surface tensions in the monolayer and the bilayer at the annulus region.

As a final test, proteoliposomes (liposomes containing membrane proteins or channels) containing the mechanically-activated channel MscL (V23T mutant) were added to the original lipid solution and incorporated into the DIB membranes as originally described by Najem *et al.* (Figure 8)³⁴. MscL is a large-conductance tension-gated protein that forms a stretch-activated channel upon insertion into a lipid bilayer membrane³⁵. V23T MscL responds to stress or tension (~ 6 -10 mN/m) in the cellular membrane by opening conductive pathways, and may be used as a biosensor to estimate the membrane areal strain through changes in the membrane conductivity³⁶. During the gating process, several temporary conductive substates are observed³⁷, consistent with high occupancy of subconductive states at low tensions in patch-clamp experiments³⁸ and in DIBs³⁴. The channel is used here in

a high-frequency mechanical oscillation case (61.5 Hz) at 50 mV, and the recorded V23T MscL gating events indicate that the membrane is experiencing high tension or stretch. The amplitude of oscillation supplied to the droplets is gradually increased until membrane failure.

Uneven droplet sizes are used for MscL activation, with the smaller droplet attached to the actuator. This smaller droplet possesses a higher internal pressure (Equation (12)), allowing for a greater deformation of the membrane as evidenced by the higher capacitive component (indicated by the greater slope of the mechanoelectric current with respect to voltage, predicted by Equation (3)) of the current shown in Figure 7.b. The overall deformation of the membrane may be tuned by the droplet composition, and this is exploited here to maximize the gating activity of MscL.

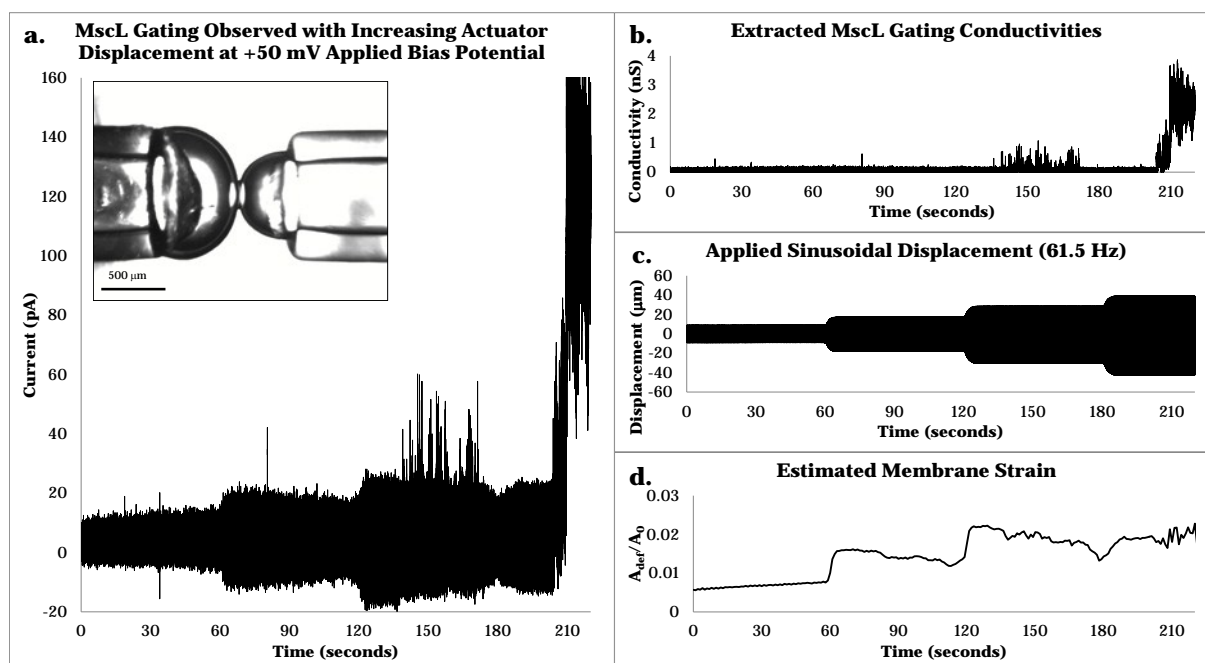


Figure 8 – Incorporation of the stretch-activated channel MscL V23T in the membrane formed by droplets of unequal sizes. a) The displacement is gradually increased as seen in c) and a 50 mV DC potential is applied to estimate the membrane conductivity. b) The mechanoelectric current is subtracted from the original experimental current seen in a), allowing for the isolation of the gating events, showing partial and full MscL gating events. c) The peak-to-peak displacement of the piezoelectric oscillator (61.5 Hz) is gradually increased through the experiment, increasing the voltage to the actuator by 1 V every minute. d) The membrane strain is estimated by calculating the required change in capacitance for the measured current and comparing it to the original membrane area.

MscL gating events are recorded as changes in the membrane conductivity. The conductivity of the membrane is calculated by subtracting the mechanoelectric current components from the summed experimental current in Figure 8.a. This isolates the MscL gating events from the membrane mechanoelectrical response, and dividing the current by the supplied 50 mV DC transmembrane potential provides the overall membrane conductance. Temporary MscL conductive substates are recorded as the actuator displacement increases. At peak displacement, MscL begins to fully gate and remains open until membrane failure. The oscillation frequency is high enough to avoid bilayer growth as shown previously, and the method of activation is through membrane stretch and strain.

The strain experienced by the membrane is estimated by the total mechanoelectric current, with the assumption that the mechanoelectric current with the supplied 50 mV transmembrane potential is primarily capacitive (Equation (5)). The mechanoelectric current is integrated from PSD analysis as described previously, and does not contain the MscL gating behaviours. The membrane strain reaches a plateau once the MscL channels begin to fully gate, and no longer increases with the actuator displacement. This indicates that there is an

upper limit to the mechanoelectrical behaviour which is governed by a critical membrane strain. The maximum strain achievable in the membrane prior to failure is roughly 2%, which aligns with the critical areal strains observed by Needham in his studies on the mechanical properties of membranes³⁹, further confirming the elastic nature of the membrane deformation.

Conclusions

The droplet-interface bilayer approach allows for a great deal of control over the membrane dimensions and properties. Displacement of the constitutive droplets is linked to variations in the properties of the interfacial membrane, and this provides a useful tool for characterizing membrane asymmetry and the fine electrostatic structure of the membrane. These electrostatic structures may also prove useful for signalling applications involving the microfluidic membranes.

At high frequencies of oscillation the membrane deforms elastically, producing a flexoelectric signal related to the bending and curvature of the interfacial membrane. This signal

represents the polarization of the membrane due to compression and extension of the charged groups and dipoles of the lipid molecules, and this signal may be generated independently of the voltage-clamped environment. In addition, the membrane deformation was significant enough to drive the activation of tension-gated channels within the membrane, allowing for further mechanotransduction possibilities within these DIB membranes.

Experimental Details

The work presented here uses the DIB approach for the creation of lipid membranes. The primary lipids selected for the membrane are 1,2-diphytanoyl-*sn*-glycero-3-phosphocholine (DPhPC) from Avanti Polar Lipids. DPhPC was selected due to its durability, impermeability, and stability across a wide range of conditions^{40, 41}. Buffer solutions are prepared using 500 mM KCl (Sigma Aldrich) with 10 mM MOPS (Sigma Aldrich). Lipids in powder form are hydrated with the buffer solution at concentrations of 2 mg/mL, and these liposomes are extruded repeatedly through 0.1 μ m filters for uniform liposome size. The droplets containing the liposomes are directly deposited into the tips of 1 mm O.D. capillary tubes (World Precision Instruments) containing Silver-Chloride/Silver (AgCl/Ag) electrodes encased in cured polyethylene glycol dimethylacrylate (PEG-DMA) hydrogels (Polysciences) as shown in Figure 1.e.

The liposome-containing aqueous droplets readily adhere to the hydrogels contained within the capillary tubes, providing a mechanical linkage between the droplets and manual micromanipulators (Burleigh) as shown in Figure 1.c. The liposomes gradually coat the aqueous droplets in a uniform lipid monolayer (3-5 minutes), after which the droplets are brought into contact to form a lipid bilayer at their interface. All experiments were performed within a hexadecane (Sigma Aldrich) reservoir placed on the stage of a Zeiss Axioskop on a vibration isolation table (Newport) within a Faraday cage. Figure 1.c was taken with squalene (Sigma Aldrich) in place of hexadecane to enable larger membrane formation for illustration purposes. Images were taken through use of an attached AxioCam (Zeiss).

Electrical control and recordings are provided by connecting the hydrogel-embedded AgCl/Ag electrodes to an Axopatch 200b and Digidata 1550 (Molecular Devices). Any changes in the membrane qualities through the applied mechanical deformation is translated into an experimentally observable current by the amplifier, compensating for shifts in the measured voltage and ensuring that the voltage remains clamped at the desired clamped value. Experimental data is extracted and filtered for better analysis and noise reduction. Mechanical control is provided by the rigid capillary tube attached to the ground electrode or ground droplet. A piezoelectric stack actuator (Physik Instrumente) is attached to the arm of the manual micromanipulator (Burleigh), and the displacement of the actuator is controlled by a sweep generator (Agilent). With this approach, the frequency and

amplitude of the applied deformation may be controlled. The oscillating capillary tube is suspended in the oil bath without making contact with the substrate itself to ensure minimal vibration is transmitted from the oscillator to the patch-clamp amplifier headstage.

DPhPC proteoliposomes containing V23T mutant MscL channels were prepared as discussed previously by Najem *et al.*^{34, 42}. The MscL-containing proteoliposomes were then mechanically extruded through 0.1 μ m filters (Avanti) upon arrival in the laboratory at Virginia Tech to eliminate any gradual aggregation, and diluted four-fold with the DPhPC liposomes prior to membrane formation to avoid excess channel concentrations in the membrane.

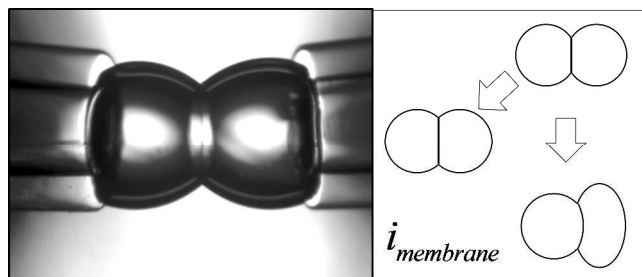
Acknowledgements

The authors would like to graciously acknowledge the funding support of NSF MCB grant #1244014 and AFOSR BRI grant #FA9550-12-1-0464 well as the generosity of Dr. Wally Grant (Virginia Tech) and the use of his laboratory equipment and manipulators.

Notes and references

1. H. Bayley, B. Cronin, A. Heron, W. L. Hwang, R. Syeda, J. Thompson and M. Wallace, *Molecular BioSystems*, 2008, **4**, 1191-1208.
2. M. A. Holden, D. Needham and H. Bayley, *Journal of the American Chemical Society*, 2007, **129**, 8650-8655.
3. K. Funakoshi, H. Suzuki and S. Takeuchi, *Analytical chemistry*, 2006, **78**, 8169-8174.
4. M. A. Holden, *Methods in Cell Biology*, 2015.
5. Y. Elani, X. Niu and O. Ces, *Lab on a chip*, 2012, **12**, 3514-3520.
6. C. Stanley, K. Elvira, X. Niu, A. Gee, O. Ces and J. Edel, *Chemical communications*, 2010, **46**, 1620-1622.
7. G. Villar, A. D. Graham and H. Bayley, *Science*, 2013, **340**, 48-52.
8. S. Sarles and D. Leo, *Smart Mater Struct*, 2011, **20**, 1-12.
9. G. Maglia, A. J. Heron, W. L. Hwang, M. A. Holden, E. Mikhailova, Q. Li, S. Cheley and H. Bayley, *Nature nanotechnology*, 2009, **4**, 437-440.
10. S. S. Dixit, A. Pincus, B. Guo and G. W. Faris, *Langmuir*, 2012, **28**, 7442-7451.
11. S. A. Sarles and D. J. Leo, *Analytical chemistry*, 2010, **82**, 959-966.
12. S. A. Sarles, J. D. W. Madden and D. J. Leo, *Soft Matter*, 2011, **7**, 4644-4653.
13. N. Tamaddoni, E. C. Freeman and S. A. Sarles, *Smart Materials and Structures*, 2015, **24**, 065014.
14. A. Petrov and V. Sokolov, *European Biophysics Journal*, 1986, **13**, 139-155.
15. A. L. Ochs and R. M. Burton, *Biophysical Journal*, 1974, **14**, 473-489.
16. P. K. Zhang, AM; Sachs, F, *Letters to Nature*, 2001, **413**.
17. B. Harland, W. E. Brownell, A. A. Spector and S. X. Sun, *Physical Review E*, 2010, **81**, 031907.

18. F. Ahmadpoor, Q. Deng, L. Liu and P. Sharma, *Physical Review E*, 2013, **88**, 050701.
19. T. Hellweg and D. Langevin, *Physical Review E*, 1998, **57**, 6825.
20. A. L. Hodgkin, A. Huxley and B. Katz, *The Journal of Physiology*, 1952, **116**, 424-448.
21. M. A. Creasy, E. C. Freeman, M. K. Philen and D. J. Leo, *Journal of Intelligent Material Systems and Structures*, 2014, 1045389X14536004.
22. S. McLaughlin, *Current topics in membranes and transport*, 1977, **9**, 71-144.
23. G. Cevc, *Biochimica et Biophysica Acta*, 1990, **1031**, 311.
24. S. McLaughlin, *Annual review of biophysics and biophysical chemistry*, 1989, **18**, 113-136.
25. K. Gawrisch, D. Ruston, J. Zimmerberg, V. Parsegian, R. Rand and N. Fuller, *Biophysical journal*, 1992, **61**, 1213-1223.
26. F. Zhou and K. Schulten, *The Journal of Physical Chemistry*, 1995, **99**, 2194-2207.
27. H. Brockman, *Chemistry and physics of lipids*, 1994, **73**, 57-79.
28. H. Yamins and W. Zisman, *The Journal of Chemical Physics*, 1933, **1**, 656-661.
29. J. Najem, M. Dunlap, I. Rowe, E. Freeman, J. Grant, S. Sukharev and D. Leo, *Submitted to ACS Nano*, 2015.
30. W. L. Hwang, M. Chen, B. d. Cronin, M. A. Holden and H. Bayley, *Journal of the American Chemical Society*, 2008, **130**, 5878-5879.
31. A. Yasmann and S. Sukharev, *Langmuir*, 2014.
32. D. Morse and T. Witten, *EPL (Europhysics Letters)*, 1993, **22**, 549.
33. K. Hristova, I. Bivas, A. Petrov and A. Derzhanski, *Molecular Crystals and Liquid Crystals*, 1991, **200**, 71-77.
34. J. S. Najem, M. D. Dunlap, I. D. Rowe, E. C. Freeman, J. W. Grant, S. Sukharev and D. J. Leo, *Scientific Reports*, 2015, **5**, 13726.
35. S. Sukharev and D. P. Corey, *Science Signaling*, 2004, **2004**, re4.
36. S. SUKHAREV, *The FASEB journal*, 1999, **13**, S55-S61.
37. S. I. Sukharev, W. J. Sigurdson, C. Kung and F. Sachs, *The Journal of general physiology*, 1999, **113**, 525-540.
38. A. Anishkin, C.-S. Chiang and S. Sukharev, *The Journal of general physiology*, 2005, **125**, 155-170.
39. D. Needham and R. S. Nunn, *Biophysical Journal*, 1990, **58**, 997-1009.
40. T. Kitano, T. Onoue and K. Yamauchi, *Chemistry and physics of lipids*, 2003, **126**, 225-232.
41. K. Yamauchi, K. Doi, Y. Yoshida and M. Kinoshita, *Biochimica et Biophysica Acta (BBA)-Biomembranes*, 1993, **1146**, 178-182.
42. J. S. Najem, M. D. Dunlap, A. Yasmann, E. C. Freeman, J. W. Grant, S. Sukharev and D. J. Leo, *JoVE*, 2015, e53362.



The mechano-electrical response of membrane-based materials is examined in detail, linking the current generated through membrane deformation to the underlying membrane structure.